Supplemental material: Incipient magnetic instability in RuO_2 with random phase approximation

Diana Csontosová,[1] Kyo-Hoon Ahn,[2] and Jan Kuneš[1]

[1] *Department of Condensed Matter Physics, Faculty of Science, Masaryk University, Kotlářská 2, 611 37 Brno, Czechia*

[2] *Institute of Physics, Czech Academy of Sciences, Cukrovarnická 10, 162 00 Praha 6, Czechia*

(Dated: April 29, 2026)

I. METHODS

A. Hartree-Fock interaction term

For the Hartree–Fock (HF) solution of the Hubbard model, we perform the mean-field decomposition of Eq. (2) in the main text. We assume that the deviation of a single-particle operator $\hat{A}$ from its average $\langle A\rangle$ is small and therefore approximate the product of fluctuations as negligible.

$$\left(\hat{A}-\langle A\rangle\right)\left(\hat{B}-\langle B\rangle\right)=\hat{A}\hat{B}-\langle B\rangle\hat{A}-\langle A\rangle\hat{B}+\langle A\rangle\langle B\rangle\approx 0. \tag{1}$$

This approximation leads to the mean-field interaction Hamiltonian.

$$\begin{aligned}
H_{\mathrm{HF}} =& \sum_{\ell}\Big[U\left(\langle c^\dagger_{\ell\uparrow}c_{\ell\uparrow}\rangle c^\dagger_{\ell\downarrow}c_{\ell\downarrow}+\langle c^\dagger_{\ell\downarrow}c_{\ell\downarrow}\rangle c^\dagger_{\ell\uparrow}c_{\ell\uparrow}-\langle c^\dagger_{\ell\uparrow}c_{\ell\uparrow}\rangle\langle c^\dagger_{\ell\downarrow}c_{\ell\downarrow}\rangle\right)\\
&\quad -U\left(\langle c^\dagger_{\ell\uparrow}c_{\ell\downarrow}\rangle c^\dagger_{\ell\downarrow}c_{\ell\uparrow}+\langle c^\dagger_{\ell\downarrow}c_{\ell\uparrow}\rangle c^\dagger_{\ell\uparrow}c_{\ell\downarrow}-\langle c^\dagger_{\ell\uparrow}c_{\ell\downarrow}\rangle\langle c^\dagger_{\ell\downarrow}c_{\ell\uparrow}\rangle\right)\Big]\\
&+\sum_{\substack{\ell>m\\ \sigma}}\Big[U'\left(\langle c^\dagger_{\ell\sigma}c_{\ell\sigma}\rangle c^\dagger_{m\bar\sigma}c_{m\bar\sigma}+\langle c^\dagger_{m\bar\sigma}c_{m\bar\sigma}\rangle c^\dagger_{\ell\sigma}c_{\ell\sigma}-\langle c^\dagger_{\ell\sigma}c_{\ell\sigma}\rangle\langle c^\dagger_{m\bar\sigma}c_{m\bar\sigma}\rangle\right)\\
&\quad -U'\left(\langle c^\dagger_{\ell\sigma}c_{m\bar\sigma}\rangle c^\dagger_{m\bar\sigma}c_{\ell\sigma}+\langle c^\dagger_{m\bar\sigma}c_{\ell\sigma}\rangle c^\dagger_{\ell\sigma}c_{m\bar\sigma}-\langle c^\dagger_{\ell\sigma}c_{m\bar\sigma}\rangle\langle c^\dagger_{m\bar\sigma}c_{\ell\sigma}\rangle\right)\Big]\\
&+\sum_{\substack{\ell>m\\ \sigma}}\Big[(U'-J_H)\left(\langle c^\dagger_{\ell\sigma}c_{\ell\sigma}\rangle c^\dagger_{m\sigma}c_{m\sigma}+\langle c^\dagger_{m\sigma}c_{m\sigma}\rangle c^\dagger_{\ell\sigma}c_{\ell\sigma}-\langle c^\dagger_{\ell\sigma}c_{\ell\sigma}\rangle\langle c^\dagger_{m\sigma}c_{m\sigma}\rangle\right)\\
&\quad -(U'-J_H)\left(\langle c^\dagger_{\ell\sigma}c_{m\sigma}\rangle c^\dagger_{m\sigma}c_{\ell\sigma}+\langle c^\dagger_{m\sigma}c_{\ell\sigma}\rangle c^\dagger_{\ell\sigma}c_{m\sigma}-\langle c^\dagger_{m\sigma}c_{\ell\sigma}\rangle\langle c^\dagger_{\ell\sigma}c_{m\sigma}\rangle\right)\Big]\\
&+\sum_{\substack{\ell\neq m\\ \sigma}}\Big[J_H\left(\langle c^\dagger_{\ell\bar\sigma}c_{m\bar\sigma}\rangle c^\dagger_{m\sigma}c_{\ell\sigma}+\langle c^\dagger_{m\sigma}c_{\ell\sigma}\rangle c^\dagger_{\ell\bar\sigma}c_{m\bar\sigma}-\langle c^\dagger_{\ell\bar\sigma}c_{m\bar\sigma}\rangle\langle c^\dagger_{m\sigma}c_{\ell\sigma}\rangle\right)\\
&\quad -J_H\left(\langle c^\dagger_{\ell\bar\sigma}c_{\ell\sigma}\rangle c^\dagger_{m\sigma}c_{m\bar\sigma}+\langle c^\dagger_{m\sigma}c_{m\bar\sigma}\rangle c^\dagger_{\ell\bar\sigma}c_{\ell\sigma}-\langle c^\dagger_{\ell\bar\sigma}c_{\ell\sigma}\rangle\langle c^\dagger_{m\sigma}c_{m\bar\sigma}\rangle\right)\Big]\\
&-\sum_{\substack{\ell\neq m\\ \sigma}}\Big[J_H\left(\langle c^\dagger_{\ell\bar\sigma}c_{m\bar\sigma}\rangle c^\dagger_{\ell\sigma}c_{m\sigma}+\langle c^\dagger_{\ell\sigma}c_{m\sigma}\rangle c^\dagger_{\ell\bar\sigma}c_{m\bar\sigma}-\langle c^\dagger_{\ell\bar\sigma}c_{m\bar\sigma}\rangle\langle c^\dagger_{\ell\sigma}c_{m\sigma}\rangle\right)\\
&\quad -J_H\left(\langle c^\dagger_{\ell\bar\sigma}c_{m\sigma}\rangle c^\dagger_{\ell\sigma}c_{m\bar\sigma}+\langle c^\dagger_{\ell\sigma}c_{m\bar\sigma}\rangle c^\dagger_{\ell\bar\sigma}c_{m\sigma}-\langle c^\dagger_{\ell\bar\sigma}c_{m\sigma}\rangle\langle c^\dagger_{\ell\sigma}c_{m\bar\sigma}\rangle\right)\Big].
\end{aligned} \tag{2}$$

Indices ℓ and m iterate over orbitals and $\bar\sigma=-\sigma$. In the resulting expression, the odd lines represent the Hartree terms, while the even lines correspond to the Fock terms (exchange channel). The HF self-energy Σ_{HF} is given by the matrix elements of H_{HF}, while the terms producing a constant energy shift, $\langle\cdot\rangle\langle\cdot\rangle$, are omitted.

B. Derivation of RPA bubble

The Lehmann representation of the Green's function reads

$$G_{\alpha s,\gamma s'}(\mathbf{k}, i\nu_n) = \int \mathrm{d}E' \frac{A_{\alpha s,\gamma s'}(\mathbf{k}, E')}{i\nu_n - E'}. \tag{3}$$

This expression is inserted into the definition of the lattice bubble expressed on the Matsubara axis[1,2]:

$$\begin{aligned}\chi_0^{\alpha\beta s,\gamma\delta s'}(\mathbf{q}, i\nu_n, i\nu_{n'}, i\omega_m) &= -\frac{1}{N_k}\sum_{\mathbf{k}} G_{\alpha s,\gamma s'}(\mathbf{k}, i\nu_n) G_{\delta s',\beta s}(\mathbf{k}+\mathbf{q}, i\nu_{n'} + i\omega_m)\delta_{nn'} \\ &= -\iint \mathrm{d}E'\mathrm{d}E'' \sum_{\mathbf{k}} A_{\alpha s,\gamma s'}(\mathbf{k}, E') A_{\delta s',\beta s}(\mathbf{k}+\mathbf{q}, E'') \\ &\times \frac{1}{i\nu_n - E'} \frac{1}{i\nu_n + i\omega_m - E''}\delta_{nn'}.\end{aligned} \tag{4}$$

Here $A_{\alpha s,\gamma s'}$ denotes the spectral function, $i\nu_n$ and $i\omega_m$ represent fermionic and bosonic Matsubara frequencies, respectively, $\alpha, \beta, \gamma, \delta$ denote spin-orbital indices, and s, s' are site indices.

After summing over fermionic frequencies and using the standard expression for the Matsubara-frequency summation[3], we obtain

$$\begin{aligned}\chi_0^{\alpha\beta s,\gamma\delta s'}(\mathbf{q}, i\omega_m) &= -\frac{1}{N_k}\iint \mathrm{d}E'\mathrm{d}E'' \sum_{\mathbf{k}} A_{\alpha s,\gamma s'}(\mathbf{k}, E') A_{\delta s',\beta s}(\mathbf{k}+\mathbf{q}, E'') \frac{f_{\mathrm{FD}}(E') - f_{\mathrm{FD}}(E'')}{i\omega_m + E' - E''} \\ \chi_0^{\alpha\beta s,\gamma\delta s'}(\mathbf{q}, \omega) &= -\frac{1}{N_k}\iint \mathrm{d}E'\mathrm{d}E'' \sum_{\mathbf{k}} A_{\alpha s,\gamma s'}(\mathbf{k}, E') A_{\delta s',\beta s}(\mathbf{k}+\mathbf{q}, E'') \frac{f_{\mathrm{FD}}(E') - f_{\mathrm{FD}}(E'')}{\omega + E' - E'' + i\varepsilon}\end{aligned} \tag{5}$$

where the analytic continuation is performed in the last step via the substitution $i\omega_m \to \omega + i\varepsilon$, with ε infinitesimal.

By performing the substitution $\nu = E'' - E'$, renaming E' to E, and introducing the quantity $B(\mathbf{q}, \nu)$, we obtain

$$B_{\alpha\beta s,\gamma\delta s'}(\mathbf{q}, \nu) = \int \mathrm{d}E \sum_{\mathbf{k}} A_{\alpha s,\gamma s'}(\mathbf{k}, E) A_{\delta s',\beta s}(\mathbf{k}+\mathbf{q}, E+\nu)[f_{\mathrm{FD}}(E) - f_{\mathrm{FD}}(E+\nu)], \tag{6}$$

$$\chi_0^{\alpha\beta s,\gamma\delta s'}(\mathbf{q}, \omega) = -\frac{1}{N_k}\int \mathrm{d}\nu \frac{B_{\alpha\beta s,\gamma\delta s'}(\mathbf{q}, \nu)}{\omega - \nu + i\varepsilon}. \tag{7}$$

Since in HF approximation the self-energy Σ_{HF} is static and represented by a matrix of real numbers, the spectral function can be written as a sum over weighted delta functions,

$$A_{\alpha s,\gamma s'}(\mathbf{k}, E) = \sum_i w^i_{\alpha s,\gamma s'}(\mathbf{k})\delta(E - E_i(\mathbf{k})), \tag{8}$$

where $\hat{w}^i = |i\rangle\langle i|$ is the outer product of the eigenvector of $\tilde{H}_k = H_k + \Sigma_{\mathrm{HF}}$ corresponding to the eigenvalue E_i. Substituting Eq. (8) into Eq. (6), we obtain

$$\begin{aligned}B_{\alpha\beta s,\gamma\delta s'}(\mathbf{q}, \nu) &= \sum_{\mathbf{k}}\sum_{ij} w^i_{\alpha s,\gamma s'}(\mathbf{k}) w^j_{\delta s',\beta s}(\mathbf{k}+\mathbf{q}) \int \mathrm{d}E\delta(E - E_i(\mathbf{k}))\delta(E - E_j(\mathbf{k}+\mathbf{q}))[f_{\mathrm{FD}}(E) - f_{\mathrm{FD}}(E+\nu)] \\ &= \sum_{\mathbf{k}}\sum_{ij} w^i_{\alpha s,\gamma s'}(\mathbf{k}) w^j_{\delta s',\beta s}(\mathbf{k}+\mathbf{q})\delta(\nu + E_i(\mathbf{k}) - E_j(\mathbf{k}+\mathbf{q}))[f_{\mathrm{FD}}(E_i(\mathbf{k})) - f_{\mathrm{FD}}(E_i(\mathbf{k}) + \nu)]\end{aligned} \tag{9}$$

Finally, inserting Eq. (9) into Eq. (7) and applying the delta functions yields

$$\begin{aligned}\chi_0^{\alpha\beta s,\gamma\delta s'}(\mathbf{q}, \omega) = \frac{1}{N_k}\sum_{ij}\sum_{k} & w^i_{\alpha s,\gamma s'}(\mathbf{k}) w^j_{\delta s',\beta s}(\mathbf{k}+\mathbf{q})\times \\ & \frac{f_{\mathrm{FD}}(E_i(\mathbf{k})) - f_{\mathrm{FD}}(E_j(\mathbf{k}+\mathbf{q}))}{\omega + i\varepsilon + E_i(\mathbf{k}) - E_j(\mathbf{k}+\mathbf{q})}.\end{aligned} \tag{10}$$

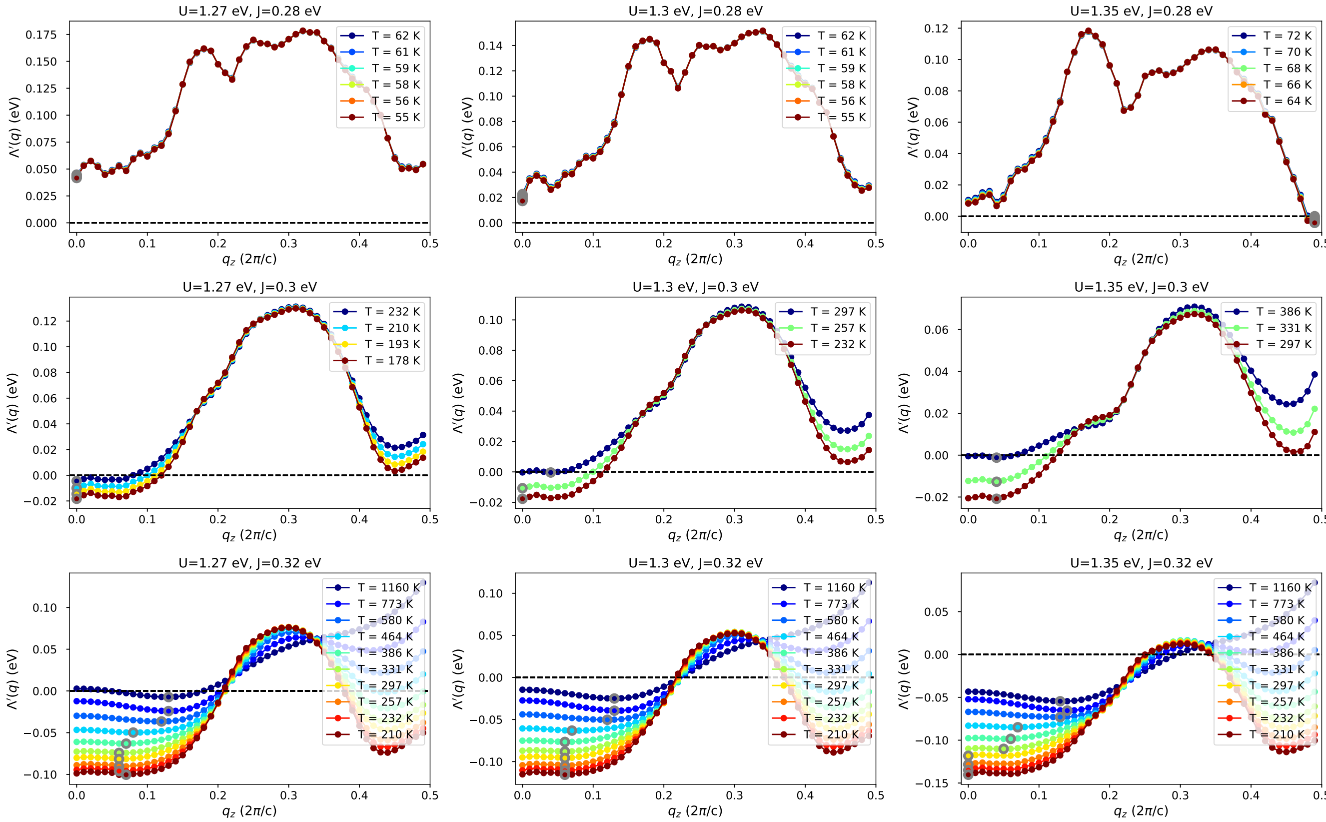

FIG. 1. The temperature dependence of the smallest eigenvalues $\Lambda'(\mathbf{q})$ of the inverse static susceptibility $\chi^{-1}(\mathbf{q})$ along the $[0, 0, q_z]$ direction for various interaction parameters in the undoped system. The gray dots show the positions of instability.

II. ADDITIONAL RESULTS

A. Temperature dependence of the instability position

In this part, we examine the temperature dependence of instability position in the parameter regime mostly below the transition temperatures, but the NM solution was enforced. In this case, the NM phase is unstable and the susceptibility may become negative. Therefore, instead of analyzing the leading eigenvalue of $\chi(\mathbf{q})$, we focus on the smallest eigenvalues $\Lambda'(\mathbf{q})$ of the inverse static susceptibility $\chi^{-1}(\mathbf{q})$.

The temperature dependence of $\Lambda'(\mathbf{q})$ for various interaction parameters in the undoped system is shown in Fig. 1. In the cases of $J_\mathrm{H} = 0.3,\mathrm{eV}$ and $J_\mathrm{H} = 0.32,\mathrm{eV}$, the value of $\Lambda'(\mathbf{q} = \Gamma)$ decreases and approaches that of $\Lambda'(\mathbf{Q} \neq \Gamma)$. For the largest U and $J_\mathrm{H} = 0.28,\mathrm{eV}$, the same trend toward $q_z = \frac{\pi}{c}$ is observed. This behavior is not present when hole doping is introduced (see Fig. 2).

B. Character of the eigenvector corresponding to the instability

To determine the nature of the instability, we analyze the absolute values of the overlaps between $\mathbf{v}(\mathbf{Q})$ and $\mathbf{Z}(\mathbf{Q})$ for one point in the phase diagram shown, in the left panel of Fig. 3. A vertical dashed line highlights three degenerate eigenvectors corresponding to the largest eigenvalue.

We compare the overlaps obtained from two types of scalar products: the standard scalar product, defined as $(\mathbf{v}, \mathbf{Z}) \equiv \sum_{ij} \overline{\mathbf{v}^{ij}} \mathbf{Z}^{ij}$ (orange crosses), and the weighted scalar product $\{\mathbf{v}, \mathbf{Z}\}$ introduced in Eq. (13) of the main text (blue dots). Since the orbital components of the eigenvectors $\mathbf{v}$ do not contribute equally, the former definition yields non-negligible overlaps with eigenvectors corresponding to different (subleading) eigenvalues. The largest overlap is 95 % and, as in the case of the latter definition, corresponds to the threefold-degenerate leading eigenvalue.

In contrast, the overlap defined in Eq. (13) suppresses these additional contributions and clearly reveals the character

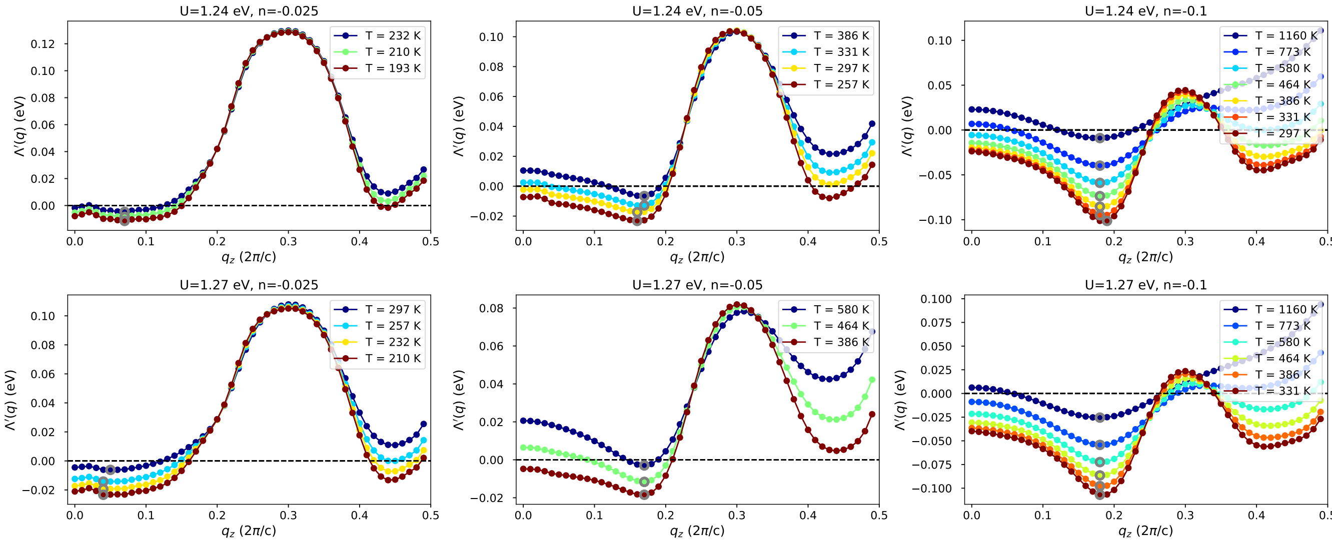

FIG. 2. The temperature dependence of the smallest eigenvalues $\Lambda'(\mathbf{q})$ of the inverse static susceptibility $\chi^{-1}(\mathbf{q})$ along the $[0, 0, q_z]$ direction for various interaction parameter U and hole doping n. The Hund's coupling is fixed at $J_{\mathrm{H}} = 0.3\,\mathrm{eV}$. The gray dots show the positions of instability.

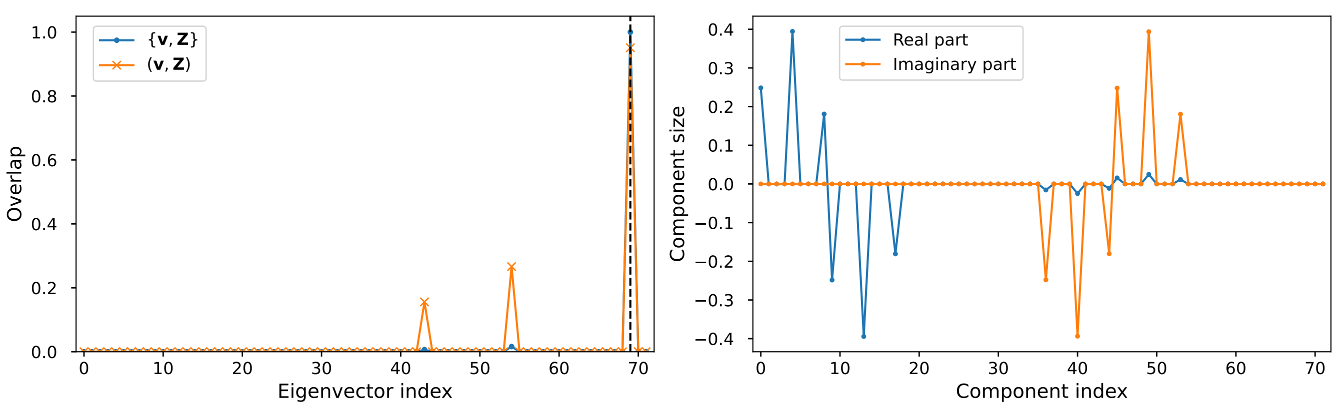

FIG. 3. The absolute values of the overlaps of the eigenvectors $\mathbf{v}_i$ of the static susceptibility $\chi(\mathbf{Q})$ at the ordering vector $\mathbf{Q}$ with the Zeeman splitting $\mathbf{Z}$ (left). Components of the eigenvector with the largest overlap (right). The component indices of eigenvector with dominant contribution are defined in the text. The parameters of the data point are: $U = 1.35\,\mathrm{eV}, J_H = 0.28\,\mathrm{eV}, n = 0, T = 77\,\mathrm{K}$ and corresponding order vector is $\mathbf{Q} = (0, \frac{2\pi}{a}, 0.48\frac{2\pi}{c})$.

of the instability. The dominant overlap (blue dots), approximately 99 %, belongs to one of the three-fold degenerate leading eigenvalues, which proves the magnetic character of the instability.

The character of the dominant eigenvector is shown in the right panel of Fig. 3. The eigenvector has real components on site 1 and almost purely imaginary components on site 2, indicating a relative rotation of the local magnetic moments on two sublattices by 90 deg. The indices of the non-negligible contributions on the x axis represent the operators

$$\{n_{x^2-y^2\uparrow 1}, n_{yz\uparrow 1}, n_{zx\uparrow 1}, n_{x^2-y^2\downarrow 1}, n_{yz\downarrow 1}, n_{zx\downarrow 1},$$
$$n_{x^2-y^2\uparrow 2}, n_{yz\uparrow 2}, n_{zx\uparrow 2}, n_{x^2-y^2\downarrow 2}, n_{yz\downarrow 2}, n_{zx\downarrow 2}\}.$$

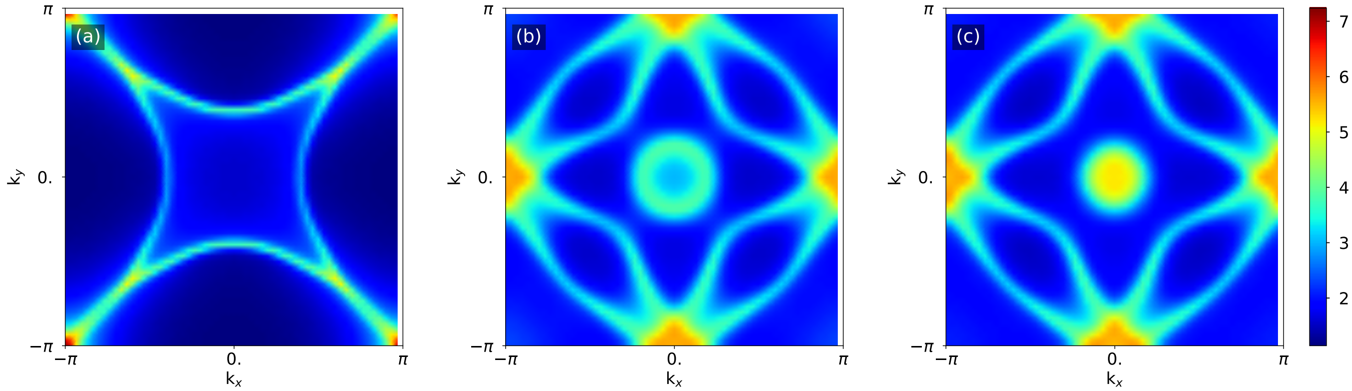

FIG. 4. Momentum-resolved contribution to the leading eigenvalue of static bubble $\tilde{\chi}_0(\mathbf{Q},\mathbf{k})$ at $\mathbf{Q} = (0, 2\pi, 0)$. The cuts are chosen to highlight the hot spots in the band structure that may be responsible for magnetic ordering at (a) $k_z = 0.35625$, (b) $k_z = 0.25$, and (c) $k_z = 0.24$ (in units of $\frac{2\pi}{c}$).

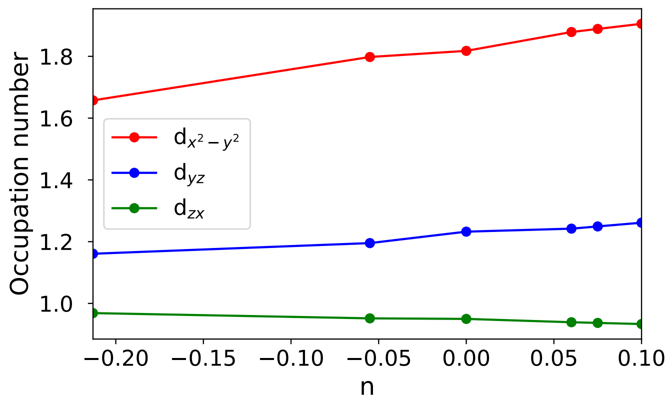

FIG. 5. The occupation numbers as a function of and doping n at $T = 773\,\mathrm{K}$. The positive (negative) values of n represent electron (hole) doping.

C. Bubble

The k-resolved static spin bubble $\tilde{\chi}_0(\mathbf{Q},\mathbf{k})$ at $\mathbf{Q} = (0, \frac{2\pi}{a}, 0)$ is shown in Fig. 4. We plot the dependencies at $k_z = 0.35625$, $k_z = 0.25$, and $k_z = 0.24$ (in the units of $\frac{2\pi}{c}$). The maxima, with values 7.236, 5.636, 5.166 and 5.715, are located around points K_2, K_4, K_5 and $(0, 0.5\frac{2\pi}{a}, 0.25\frac{2\pi}{c})$, respectively. The position of the maximal contribution to $\tilde{\chi}_0(\mathbf{Q},\mathbf{k})$ is in the contradiction with the one found in Ref.[4].

D. Occupation numbers of doped system

In this section, we show the evolution of the occupation numbers $n_{i\uparrow} + n_{i\downarrow}$ with doping and temperature, where i denotes the orbital index. With electron doping, the electrons are distributed quite evenly among the orbitals. In contrast, holes predominantly occupy the $d_{x^2-y^2}$ orbitals, leading to an enhancement of the magnetic moment with hole doping.

E. Magnon spectra

Finally, we show the magnetic excitations in RuO_2 for various values of U, with fixed $J_H = 0.3\,\mathrm{eV}$ and $T = 297\,\mathrm{K}$. The imaginary part of the $\chi_{xx}(\omega, \mathbf{q})$ component of the dynamic susceptibility is presented in Fig. 6. For all U values

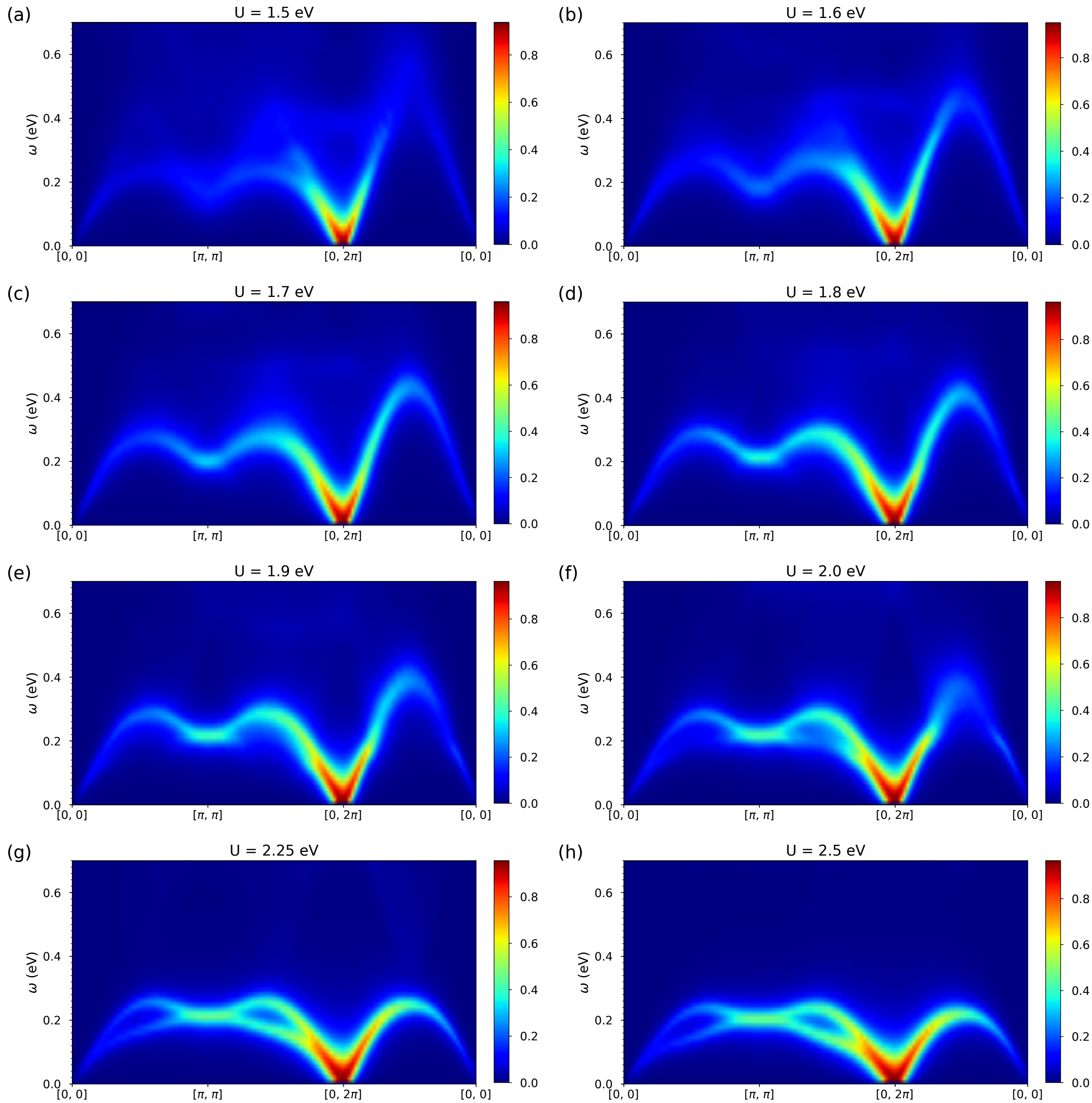

FIG. 6. Imaginary part of the $\langle S_x S_x \rangle_\omega$ component of the dynamic susceptibility, showing the magnetic excitations for various values of U and their corresponding magnetic moments: (a) $m = 1.0\,\mu_\mathrm{B}$, (b) $m = 1.24\,\mu_\mathrm{B}$, (c) $m = 1.41\,\mu_\mathrm{B}$, (d) $m = 1.51\,\mu_\mathrm{B}$, (e) $m = 1.57\,\mu_\mathrm{B}$, (f) $m = 1.61\,\mu_\mathrm{B}$, (g) $m = 1.70\,\mu_\mathrm{B}$, (h) $m = 1.75\,\mu_\mathrm{B}$.

considered, the magnon spectra exhibit a linear Goldstone mode at $\mathbf{Q} = (0, \frac{2\pi}{a}, 0)$. The unfolding procedure was applied. For clarity, we plot $\dfrac{\mathrm{Im}(\chi_{xx})}{\mathrm{Im}(\chi_{xx}) + C}$, where $C = 15$, to enhance the visibility of the spectral structure.

A splitting of the magnon spectra emerges for $U > 2.0\,\mathrm{eV}$, consistent with the findings of Šmejkal *et al.*[5], who employed a Heisenberg model to describe magnetic excitations. It arises from the asymmetric χ^{+-} and χ^{-+} components of the susceptibility representing the magnon branches with different chirality (see Figs. 7 and 8).

As U decreases, the split feature vanishes, and the dispersion resembles that of a conventional antiferromagnet.

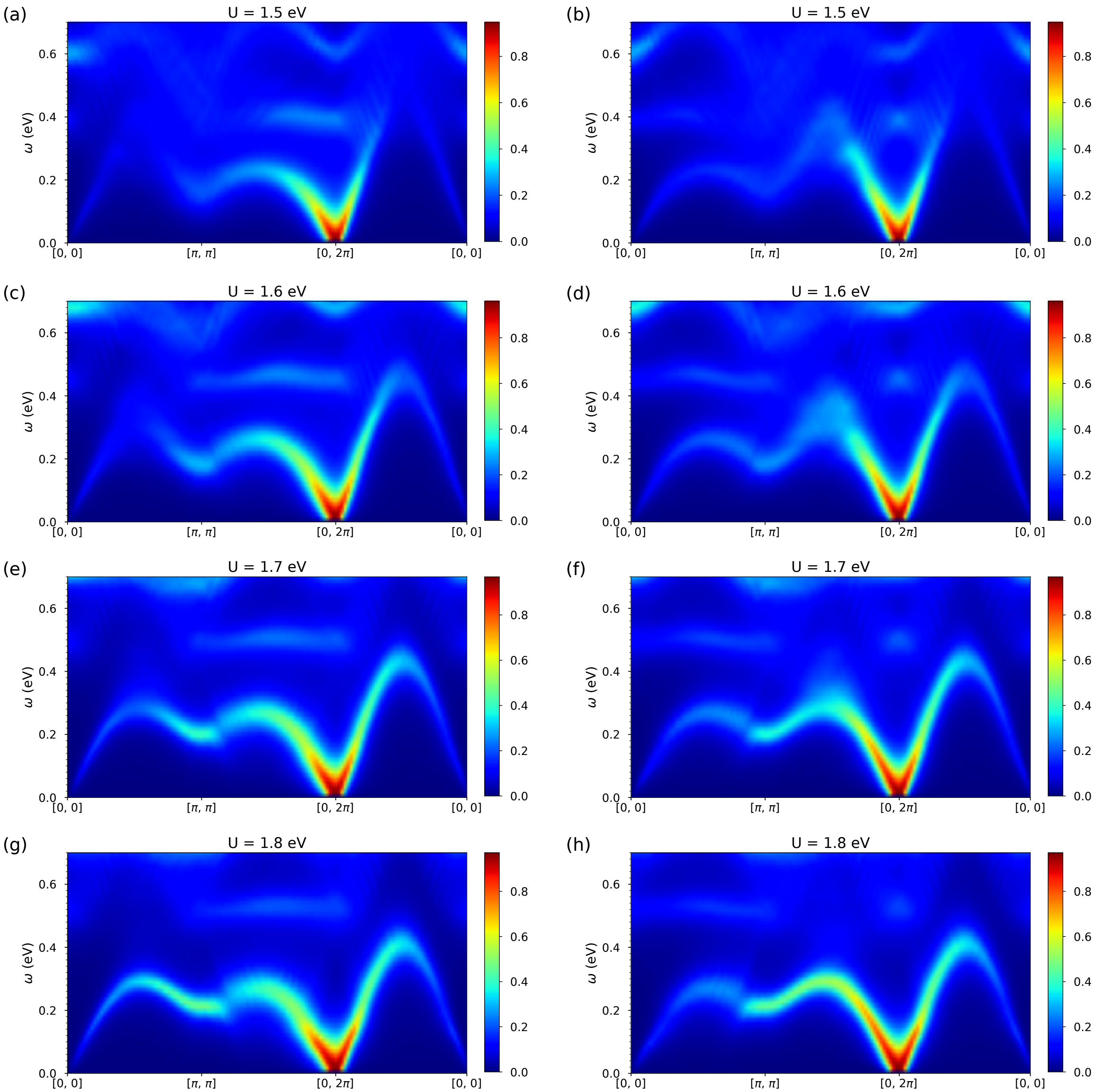

FIG. 7. Imaginary part of the (a), (c), (e), (g) χ^{+-} and (b), (d), (f), (h) χ^{-+} components of the dynamic susceptibility for various values of U.

As U decreases, the magnon bandwidth increases and the magnon splitting becomes obscured by the overlap of the upper branch with the particle-hole continuum accompanied by pronounced damping.

[1] L. Boehnke, H. Hafermann, M. Ferrero, F. Lechermann, and O. Parcollet, Phys. Rev. B **84**, 075145 (2011).
[2] J. Kuneš, Phys. Rev. B **83**, 085102 (2011), arXiv:1010.3809.
[3] G. D. Mahan, *Many-Particle Physics*, 2nd ed., Physics of solids and liquids (Springer US, Boston, MA, 2000) p. 785,

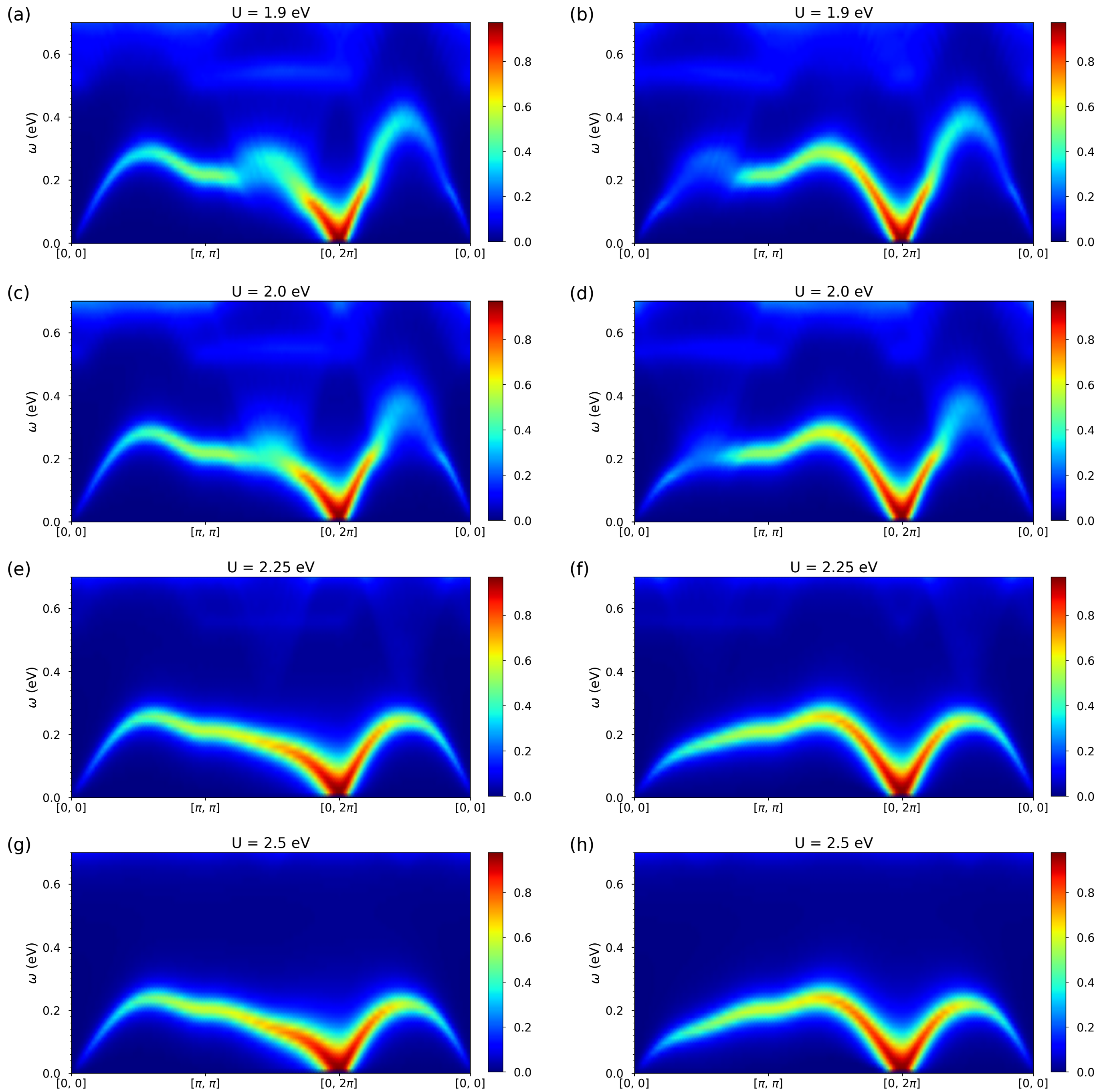

FIG. 8. Imaginary part of the (a), (c), (e), (g) χ^{+-} and (b), (d), (f), (h) χ^{-+} components of the dynamic susceptibility for various values of U.

arXiv:arXiv:1011.1669v3.

[4] T. Berlijn, P. C. Snijders, O. Delaire, H.-D. Zhou, T. A. Maier, H.-B. Cao, S.-X. Chi, M. Matsuda, Y. Wang, M. R. Koehler, P. R. C. Kent, and H. H. Weitering, Phys. Rev. Lett. **118**, 077201 (2017).

[5] L. Šmejkal, A. Marmodoro, K.-H. Ahn, R. González-Hernández, I. Turek, S. Mankovsky, H. Ebert, S. W. D'Souza, O. c. v. Šipr, J. Sinova, and T. c. v. Jungwirth, Phys. Rev. Lett. **131**, 256703 (2023).